Life Sciences 319 (2023) 121537

Contents lists available at ScienceDirect

Life Sciences

journal homepage: www.elsevier.com/locate/lifescie

Ketotifen is a microglial stabilizer by inhibiting secretory vesicle acidification

María Pilar Ramírez-Ponce [a], Juan Antonio Flores [b], Lorenzo Barrella [a], Eva Alés [a,*]

[a] Dpto. de Fisiología Médica y Biofísica, Facultad de Medicina, Universidad de Sevilla, Spain
[b] Dpto. de Bioquímica Médica y Biología Molecular e Inmunología, Facultad de Medicina, Universidad de Sevilla, Spain

ARTICLE INFO

Keywords:
Microglia
Acidification
Calcium signaling
Exocytosis
Ketotifen
Secretory vesicles
Neuroinflammation

ABSTRACT

Aims: Microglia survey the brain environment by sensing alarm signals to provide the first line of defense against injury or infection after which they acquire an activated phenotype, but they also respond to chemical signals sent from brain mast cells, sentinels of the immune system, when these are degranulated in response to noxious agents. Nevertheless, excessive microglia activation damages the surrounding healthy neural tissue causing progressive loss of neurons and inducing chronic inflammation. Thus, it would be of intense interest the development and application of agents which prevent mast cell mediator release and inhibit the actions of such mediators once released on microglia.

Main methods: Fluorescence measurements of *fura*-2 and quinacrine were used to measure intracellular Ca^{2+} signaling and exocytotic vesicle fusion in resting and activated microglia.

Key findings: We show that treatment of microglia with a cocktail of mast cell mediators induces microglia activation, phagocytosis, and exocytosis, and reveal by the first-time microglia undergo a phase of vesicular acidification just before the exocytotic fusion occurs. This acidification is an important process for vesicular maturation and contributes with ~25 % to the content that the vesicle can store and later release by exocytosis. Pre-incubation with ketotifen, a mast cell stabilizer and H1R antagonist completely abolished histamine-mediated calcium signaling and acidification of microglial organelles, and concomitantly reduced the discharge of vesicle contents.

Significance: These results highlight a key role for vesicle acidification in microglial physiology and provide a potential therapeutic target for diseases related to mast cell and microglia-mediated neuroinflammation.

1. Introduction

Microglial cells are resident tissue macrophages of the CNS and function as the first defense in the brain. These cells are characterized by the presence of dense branching processes and scan the neighboring microenvironment for extracellular threats. Once a danger signal is detected, they are activated by dramatically changing their morphology, migrating to the site of the injury, and proliferating [1,2]. In addition, they phagocytose dying cells, eliminate threatening agents and other debris, and/or secrete inflammatory and trophic factors to maintain homeostasis and neuronal survival. However, when overactivated in severe injury or neurodegenerative diseases, microglia cells acquire a neurotoxic role, releasing harmful molecules such as interleukin (IL)-1β, IL-6, TNF-α, nitric oxide, reactive oxygen species (ROS) and contribute to the progression of neurodegeneration and inflammation [3,4]. Therefore, modulation and inhibition of microglial overactivation may provide a therapeutic target to improve the treatment of neurodegenerative diseases.

Mast cells (MCs), known for their role in allergic diseases, reside close to microglia and neurons in the CNS [5,6] and their presence increase under pathophysiological conditions, such as in Alzheimer's disease [7,8], responding to injurious stimuli faster than microglia [9]. MCs store numerous pro-inflammatory mediators, such as histamine, in secretory granules and can secrete them upon activation [10,11]. MC degranulation can directly induce microglia activation with the subsequent production of ROS and pro-inflammatory factors and can aggravate LPS-induced neuroinflammation [12,13]. Furthermore, activated brain MCs contribute to postoperative cognitive dysfunction by evoking microglial activation and neuronal apoptosis [12]. Otherwise, stabilization of MCs by cromolyn inhibits LPS-induced neuroinflammation and

* Corresponding author at: Dpto. Fisiología Médica y Biofísica, Facultad de Medicina, Universidad de Sevilla, Av. Sánchez Pizjuán 4, 41009 Sevilla, Spain.
E-mail address: eales@us.es (E. Alés).

https://doi.org/10.1016/j.lfs.2023.121537
Received 26 January 2023; Received in revised form 22 February 2023; Accepted 24 February 2023
Available online 2 March 2023

memory impairment [14] and improves long-term cognition [15]. Therefore, inhibition of MC activation should also be neuroprotective.

MC dependent microglial activation is largely mediated by histamine [12,16,17]. Histamine induces microglia activation and dopaminergic neuronal toxicity by activating the H1 receptor [18] and triggers microglial phagocytosis and ROS production through histamine receptor H1R and H4R activation. Antagonists of H1R have beneficial effects against microglia-mediated oxidative stress and neurotoxicity [18,19]. However, it is unknown how histamine-mediated activation of microglia affects the exocytotic release of secretory vesicles, which is a crucial process that determines the secretion of different cytokines, chemokines, and other soluble factors that build up and maintain the inflammatory response [20].

Ketotifen is a MC stabilizer and H1R receptor antagonist [21]. While it inhibits MC degranulation may also prevent the direct effect of histamine on microglial activation. In this work, we examine the role of the H1R in both resting and activated microglia and find that ketotifen could reverse microglial overactivation. This investigation demonstrates that regulation of the pH of secretory vesicles in microglia may represent a novel mechanism that contributes to modulation of inflammatory mediator secretion and reveals an unsuspected effect of ketotifen to diminish the acidification of the secretory organelles and the discharge of the vesicle content.

2. Materials and methods

2.1. Microglia culture

Regular primary mixed glia cultures were prepared from the cerebral cortices of newborn Wistar rats (P2-P4) which were subjected to mechanical dissociation as described [17]. All procedures were approved by the Institutional Committee of the University of Seville for the Care and Use of Animals. Animal handling was carried out in accordance with Directives 86/609/EEC and 2010/63/EU for the Care and Use of Laboratory Animals. Briefly, after filtering cells through a filter nylon mesh of 100 μm, the cells obtained were seeded in Dulbecco's modified Eagle's medium (DMEM)/F12 with 20 % of inactivated foetal bovine serum (FBS, Hyclone) at a density of 300,000 cells/ml on 15 mm-diameter cover glass and maintained at 37 °C in a humidified atmosphere of 5 % CO_2/95 % air. Culture medium was replaced after 5 days in vitro (DMEM/F12 and 10 % inactivated FBS) and changed every 3 days. The cultures showed a heterogeneous population of cells mainly composed of microglia and astrocytes (performing of mild trypsinization procedure for microglial enrichment was avoided, as we observed it promotes in vitro activation of microglia). The coverslips that showed a higher density of isolated microglia were selected according to morphological criteria. The morphological selection of cells was correlated with iba-1 staining, a selective marker of microglia. Cells were used between 14 and 21 days in culture. Cells with more than three extensions were selected as ramified microglia.

2.2. Cocktail of mast cell mediators

A cocktail of MC mediators (Mast cell Conditioned Medium, MCM) was prepared as previously described [22]. Briefly, 1×10^6 purified MCs obtained after a 70 % Percoll purification were resuspended in 1 ml of basal Locke solution containing 140 mM NaCl, 10 mM HEPES, 3 mM KOH, 2 mM $CaCl_2$, 1 mM $MgCl_2$ and 10 mM glucose (pH 7.3, adjusted with NaOH). Cells, at a concentration of 10^6/ml, were placed in a pre-warmed thermomixer (Eppendorf) for 1 h at 53 °C with moderate agitation (600 rpm). MCs degranulation was verified by visual inspection under a microscope. The MCM was obtained from the supernatant after centrifugation of the MCs solution at 200 ×*g* for 5 min. Supernatant was aliquoted (50 μl) and stored at −80 °C until use.

2.3. Enzyme-linked immuno-sorbent assay (ELISA)

The expression of histamine and ATP levels in MCM were quantified with a commercial Beckman Coulter ELISA kit (IMMUNOTECH – Prague, Czech Republic) and an ATP assay kit (SIGMA), respectively following the manufacturer's instructions. All samples were run in duplicate.

2.4. Recordings of $[Ca^{2+}]_i$ signal

The changes in $[Ca^{2+}]_i$ of microglial cells in response to different stimuli were monitored by dual excitation microfluorimetry. Microglial cells were incubated in Locke external solution containing Fura-2 AM 5 μM (Molecular Probes) and Pluronic F-127 0.004 %, (Sigma) for 45 min at 37 °C in the dark. Later, cells were washed twice in external solution without the dye and used for imaging. The cover glass with cells loaded with Fura-2 AM was then mounted in a RC-25F perfusion chamber (Warner instruments) and placed on the microscope (AxioVert 200, Zeiss). During recordings, microglial cells were excited by a xenon light source at 360/380-nm wavelengths (exposure time, 0.5 s; data acquisition at 0.33 Hz) by means of two narrow beam band-pass filters selected by a computer-controlled wheel. The emitted fluorescence was filtered through a 520-nm filter and captured with an ORCA-R2 CCD camera (Hamamatsu Photonics). Fura-2 AM loading was generally uniform throughout the cytoplasm, and dye compartmentalization was never observed. Data were acquired and stored using the HCImage software and exported to Igor Pro (WaveMetrics) to perform analysis. All values were normalized to the basal fluorescence (baseline). The $[Ca^{2+}]_i$ signal was expressed by the ratio of fluorescence at 360 and 380 nm. The agents used to stimulate microglia were MCM, histamine 100 μM and ATP 100 nM. These products were applied by means of a pressure pulse (5 s) with a micropipette (1 μm diameter) placed approximately 100 μm to the microglial cell. All experiments were carried out at 37 °C.

2.5. Phagocytosis assay and microglia immunofluorescence

Microglial cells were treated for 48 h as follows: control (without any treatment), MCM 10 %, histamine 100 μM, ATP 10 nM. When necessary, cells were incubated with ketotifen 100 μM or PPADS (pyridoxalphosphate-6-azophenyl-2′,4′-disulfonic acid) 50 μM, a selective purinergic P2X antagonist. Later, we proceeded to the phagocytosis assay. This is as follows (with some modifications [23]). Fluorescent latex beads were used to assay phagocytosis. They were pre-opsonized in non-inactivated FBS for 1 h at 37 °C. The ratio of beads to FBS was 1:5. Beads containing FBS with DMEM/F12 with 10 % inactivated FBS were diluted to reach final concentrations of beads and FBS in DMEM/F12 of 0.01 % (*v*/v) and 0.05 % (v/v), respectively. Then, cell cultures were incubated with beads-containing medium at 37 °C for 1 h and washed thoroughly with ice-cold PBS 5 times. The cells were then fixed using 4 % PFA for 30 min at room temperature. After that, we performed iba-1 immunofluorescence. First, cells were permeabilized with 0.1 % Triton X-100 in PBS and, after adding blocking solutions for 1 h at room temperature, incubated overnight with rabbit anti-Iba1 monoclonal antibody (1:1000) (Synaptic Systems) at 4 °C. Cells were washed five times with PBS, then incubated with Alexa Fluor 555 conjugated goat anti-rabbit secondary antibody (1:500) (Molecular Probes) at room temperature for 1 h. After this, cells were washed five times with PBS and mounted on cover glasses with Fluoromont-G medium. Fluorescent images were acquired randomly using an inverted microscope (AxioVert 200, Zeiss). To visualize iba-1 staining, microglia were excited by a xenon light source at a wavelength of 552 nm (exposure time, 0.8 s); for beads, these were excited with a FITC filter at 495 nm (exposure time, 0.08 s). The emission wavelengths were 578 and 519 nm, respectively. For the study of the effects of MCM and the rest of the treatments on the number of phagocytosed beads (mean ± S.E.M.), bead-labeled cells were counted in four separate culturing procedures under the microscope with a 40×

objective. Microglial cell area, perimeter, and intensity were measured from iba-1 cell fluorescence images through automatic threshold selection (HCImage).

2.6. Imaging and analysis of quinacrine dye release

To visualize the acidic organelles of microglia, the microglia were treated with quinacrine 10 μM in Locke external solution for 10 min at 37 °C in the dark. Later, microglial cells were washed twice in external solution without the dye and used for imaging. The cover glass with quinacrine loaded cells was then mounted and transferred to the chamber for imaging under an inverted microscope with a 40× objective (Zeiss). The fluorescence images were collected every 5 s, with excitation at 472 nm and emission at 579 nm. Data analysis was performed with HCImage software (Hamamatsu). Time-lapse imaging of quinacrine fluorescence was evaluated after application of MCM. When necessary, cells were incubated with ketotifen 100 μM or bafilomycin A1 400 nM for 10 min at 37 °C before MCM application. During off-line analysis, with this same software, regions of interest (ROI), cells, or individual vesicles, were manually selected. In a typical experiment, 4 to

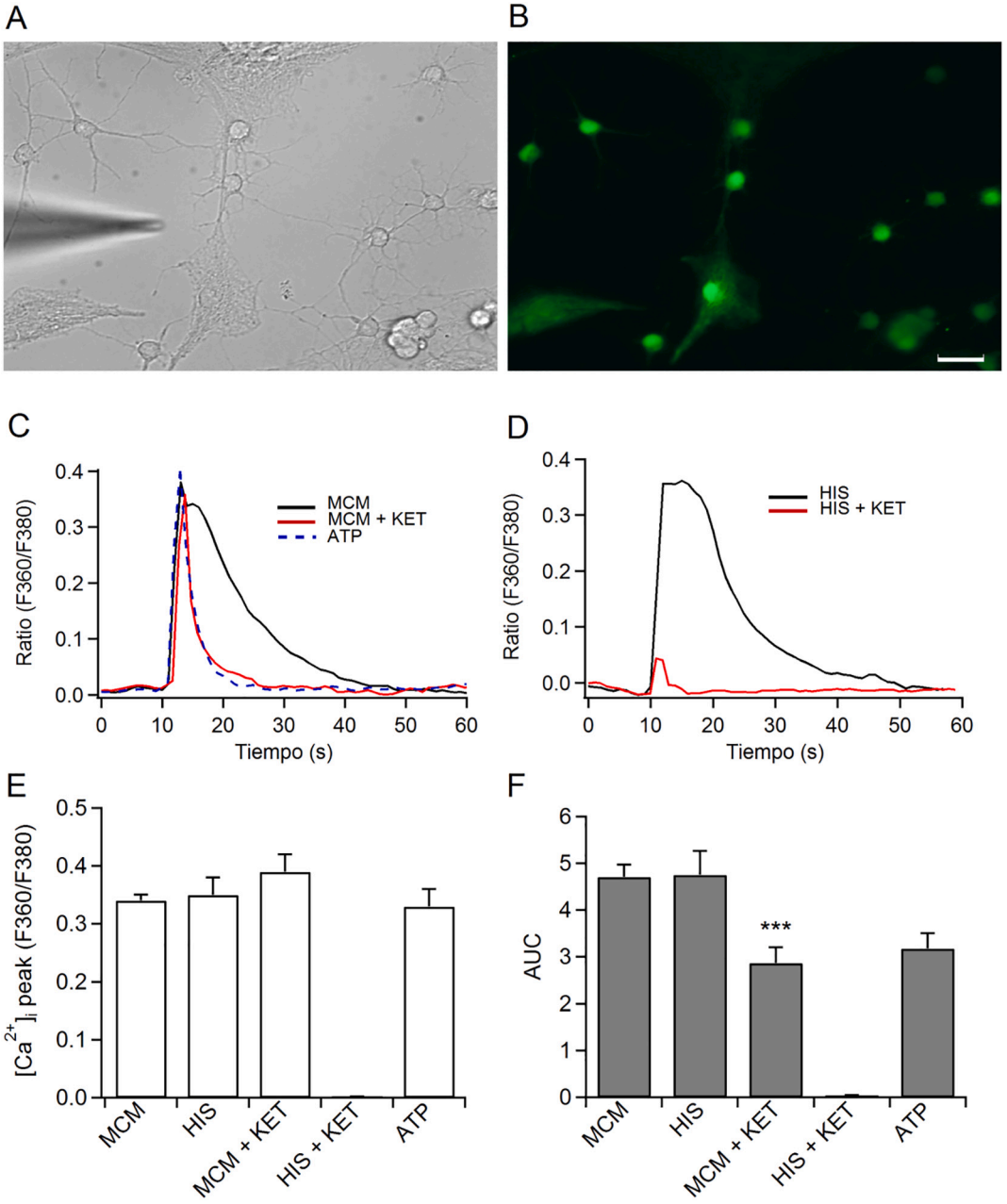

Fig. 1. Calcium imaging of microglial cells. A) Phase contrast image of rat cultured microglia with a 1 μm glass micropipette connected to a picospritzer that applies 5 s pressure ejection (2.5 psi) pulses. B) Fluorescence image showing the same cells in A, loaded with the Ca^{2+} sensitive dye Fura 2-AM. C) Representative traces of $[Ca^{2+}]_i$ transients evoked by the application of MCM (black line), MCM applied after 10 min incubation with ketotifen 100 μM (MCM + KET) (red line) and ATP 100 nM (dashed line). D) Representative traces of $[Ca^{2+}]_i$ transients evoked by application of histamine 100 μM (HIS) (black line) and histamine applied after 10 min incubation with ketotifen 100 μM (HIS + KET) (red line). E) Mean $[Ca^{2+}]_i$ peak and F) Area under curve (AUC) obtained in microglia-evoked responses by stimulation with MCM ($n = 102$), histamine 100 μM (HIS) ($n = 25$), MCM after incubation with ketotifen 100 μM (MCM + KET) ($n = 36$), histamine 100 μM after incubation with ketotifen 100 μM (HIS + KET) ($n = 13$) and ATP 100 nM (ATP) ($n = 54$). Values (mean ± S.E.M) were calculated from three independent culturing experiments. Statistically significant from MCM-treated cells (***$p < 0.001$) using Mann-Whitney rank sum test. Scale bar: 10 μm. (For interpretation of the references to colour in this figure legend, the reader is referred to the web version of this article.)

12 cells were visible in the field of view. The time course of changes in quinacrine fluorescent intensity was measured for those vesicles that retained their XY position within the ROI throughout the observation period, typically 10–20 min. Changes in the mean fluorescence intensity of each ROI were displayed in arbitrary units (au) without background subtraction. Exocytotic events were defined as decreases in ROI fluorescence of >20 % between the maximum and minimum fluorescence measured. The release fraction was calculated as the percentage of fluorescence loss in relation to the maximum fluorescence of the ROI.

2.7. Statistical analysis

Statistical analyzes were performed with the Mann-Whitney rank sum test or the Student's *t*-test (SPSS Statistics 25). All measurements were expressed as mean ± standard error of the mean (SEM) and $p < 0.05$ was considered significant.

3. Results

3.1. Calcium transients evoked by MCM in microglia are mainly due to H1R

In the present study, we stimulated cultured rat microglial cells with a pressure pulse (5 s) of MCM (Fig. 1A). This cocktail of MC mediators was obtained by heat (53 °C, 1 h). Previously, we have shown the main mediators of MCs able to evoke a calcium signal in microglia were histamine and ATP [17]. Histamine and ATP concentrations of the cocktails measured by ELISA were 263 ± 73 μM and ~ 100 nM, respectively, therefore we stimulated also with histamine 100 μM and ATP 100 nM in our experiments. Ketotifen was used because it is a H1 receptor antagonist and in addition, it can reduce the final histamine concentration in MCM by 50 % (measured by ELISA). The MCM showed a rapid and transient elevation of intracellular calcium ($[Ca^{2+}]_i$) measured by Fura-2 AM fluorescence (Fig. 1B, C). The increase in $[Ca^{2+}]_i$ evoked in microglial cells by MCM was partially inhibited by a previous incubation (10 min) with ketotifen 100 μM. As a result, a fine, sharp calcium transient resembling the signal induced by ATP was observed (Fig. 1C). However, the histamine-induced calcium signal was completely abolished by ketotifen (Fig. 1D). The MCM-induced calcium transients had a peak of 0.34 ± 0.01 and an area under curve (AUC) of 4.71 ± 0.27 that were like that induced by histamine (peak: 0.35 ± 0.03; AUC: 4.75 ± 0.51) (Fig. 1E, F). Ketotifen did not modify the maximum value of the calcium peak when stimulated with MCM (0.39 ± 0.03) but partially inhibited the AUC (2.87 ± 0.0.34). These parameters were supressed by ketotifen when histamine instead of MCM was applied. ATP showed a behavior like that obtained with MCM in the presence of ketotifen (peak: 0.33 ± 0.03; AUC: 3.18 ± 0.33) (Fig. 1E, F). Clearly, ketotifen acts to inhibit the elevation of $[Ca^{2+}]_i$ produced by activation of the H1R in microglia.

3.2. Ketotifen does not inhibit MCM-mediated microglia activation

Elevations of $[Ca^{2+}]_i$ play a vital role in the microglial activation process. Because microglial cells with a ramified morphology with long, thin processes and small cell bodies are the main responders to MCM [17], we decided to determine the number of cells that are capable of being activated in the presence of MCM (diluted down to 10 %), modifying their phenotype. Whereas in the 'resting' state these cells exhibit ramified microglia shapes and a weaker iba1 signal, a microglia-specific calcium-binding protein, when activated by histamine and MCM, cells showed an intense expression of iba1 in spindle, rod, or amoeboid-shaped cells, corresponding to activated microglia (Fig. 2A). Table 1 summarizes the average area and perimeter values obtained after treatments. Rat microglia cultures showed 22.74 ± 3.5 % of activated cells that increased to 32.95 ± 3.1 % in the presence of histamine 100 μM (Fig. 2B). MCM elevated this percentage up to 49.82 ± 5.42 %. ATP 10 nM produced up to 56 ± 4.95 % of microglia activation. This concentration of ATP was used to emulate the effects of MCM at 10 %. No changes in microglial activation by histamine were observed in a concentration range between 10 and 100 μM. Neither ketotifen nor PPADS (a purinergic P2X receptor antagonist) were able to reverse the effect of MCM (62.32 ± 5.39 % and 41.95 ± 6.24 %), suggesting that neither H1R nor P2XR are involved in microglia activation.

3.3. Ketotifen decreases phagocytosis in activated microglia

Phagocytosis was assessed using fluorescent latex beads of 1 μm diameter. MCM (10 %) and histamine 100 μM showed an increase in microsphere engulfment per cell (MCM: 4.81 ± 0.6; HIS: 4.79 ± 0.59) with respect to control cells (2.22 ± 0.22) (Fig. 2C). ATP 10 nM was also used and did not show significant differences with respect to control (2.11 ± 0.28). Incubation with ketotifen and PPADS did not significantly modify MCM-induced phagocytosis, although there was a downward trend (KET: 3.3 ± 0.4; PPADS: 4.5 ± 0.44). However, ketotifen did reduce histamine-induced phagocytosis (2.5 ± 0.3) (Fig. 2C).

To understand how cell activation and morphological changes can influence microglial functional responses, we have related phagocytosed beads per cell in ramified versus activated microglia. Phagocytosis in ramified cells was not affected by any stimulus or treatment with respect to the control, showing a low capture rate (Control: 1.24 ± 0.44; MCM: 1.4 ± 0.22; HIS: 1.52 ± 0.23; ATP: 1.15 ± 0.2; MCM + KET: 1.59 ± 0.28; MCM + PPDAS: 1.39 ± 0.27; HIS + KET: 1.92 ± 0.3) (Fig. 2D). However, the rate of phagocytosis observed in activated cells under basal conditions (control) is higher than that observed in ramified cells (3.93 ± 0.59) although it increased more than double in the presence of MCM (9.05 ± 1.25) and histamine (10.82 ± 1.51). On the contrary, ATP inhibited the number of beads per cell (2.66 ± 0.44) relative to the control. Incubation with ketotifen decreased the rate of phagocytosis under treatment with MCM (4.56 ± 0.77) and histamine (3.25 ± 0.58). The overall phagocytosis rate (ramified + activated) increased respect to the control because of the higher number of MCM-activated cells did not reduce by ketotifen. Last, incubation with PPADS did not affect the phagocytosis generated by the MCM (8.77 ± 1.11) (Fig. 2E).

3.4. Effect of ketotifen on quinacrine fluorescence in activated and ramified microglia

We incubated cells with quinacrine (10 μM for 10 min at 37 °C), a fluorescent marker for acidic organelles, such as secretory granules and lysosomes for long-term imaging [24]. We measured fluorescence changes in ramified and activated cells after stimulation with MCM for 30 s through a microperfusion pipette (Fig. 3A, C). In most cells, a slow increase in fluorescence occurred to a greater or lesser extent, always preceding the subsequent loss of dye due to vesicle fusion with the plasma membrane. The time course of fluorescence resembles a wave whose amplitude is more pronounced in activated than in ramified microglia. Interestingly, the presence of ketotifen abolished this increment but the exponential loss of fluorescence was not affected (Fig. 3B, D). Fluorescence increases were not significantly different between basal and MCM-stimulated microglia (Fig. 3E). Nevertheless, the rise was greater in activated cells than in ramified ones. Preincubation with ketotifen completely inhibited the rate of rise of the quinacrine signal in both control and MCM-treated cells. Similarly, bafilomycin 400 nM (a potent and selective inhibitor of V-ATPase) almost suppressed the rise of fluorescence. Cetirizine 100 μM also produced a great inhibition. In correlation with these data, the fraction of rise in fluorescence mediated by MCM in activated cells (26.71 ± 3.7 %) was abolished completely by the presence of ketotifen (1.61 ± 0.4 %) (Fig. 3F). Likewise, the fraction of release by the exocytotic process (62 ± 3.5 %) was partially inhibited by ketotifen (49.11 ± 1.9 %) (Fig. 3F). Therefore, ketotifen inhibits the rise of fluorescence through a mechanism that seems to involve organelle acidification, and this could reduce the exocytotic response.

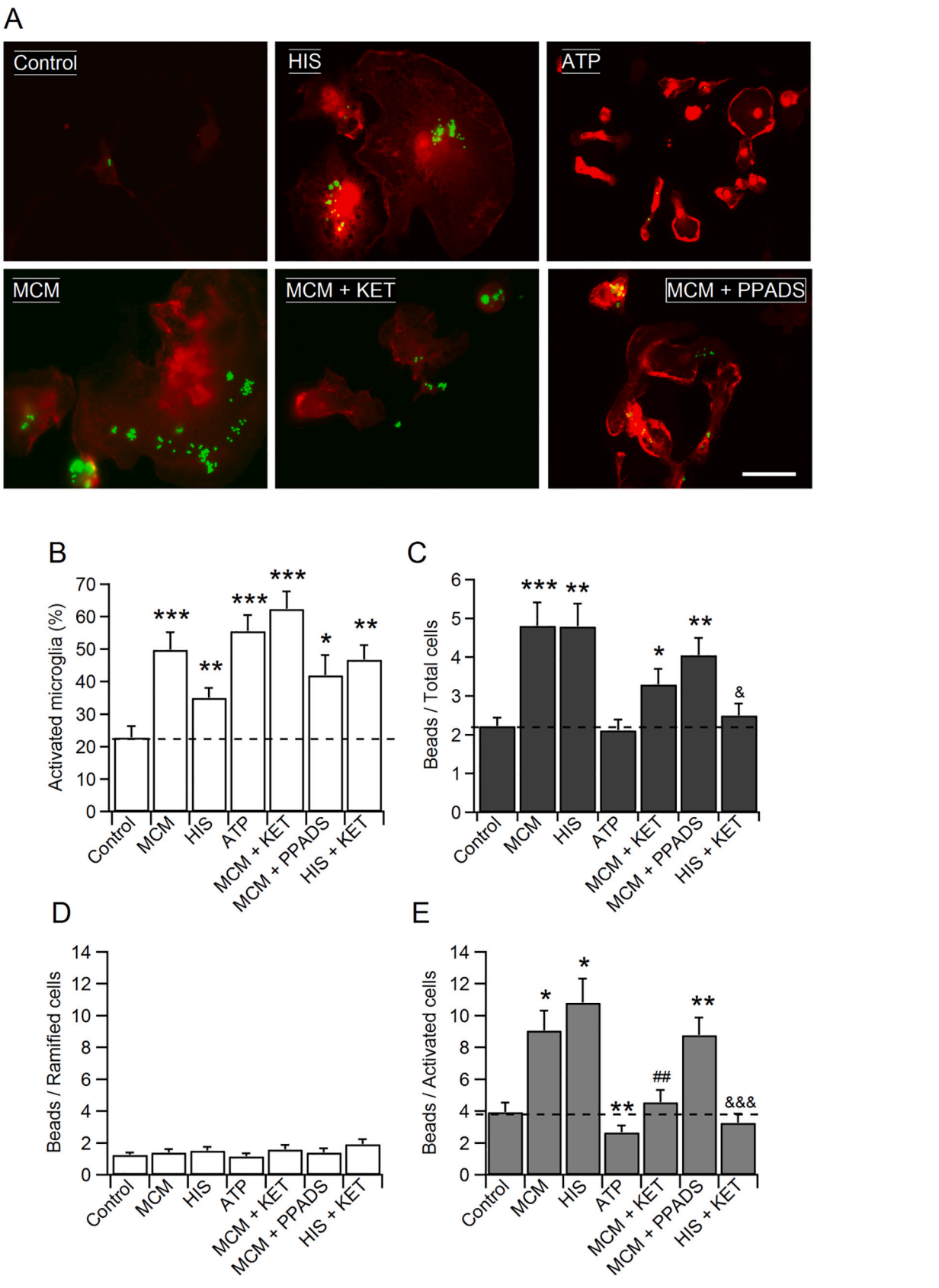

(caption on next page)

Fig. 2. Microglial activation and phagocytosis in ramified versus activated microglia. A) Representative images illustrate latex microbeads phagocytosis of iba1 positive microglial cells (red) in nontreated cells (Control) and treated cells with histamine 100 μM (HIS), ATP 10 nM, MCM, MCM after incubation with ketotifen 100 μM (MCM + KET) and MCM + PPADS. B) Percentage of cells showing an activated phenotype. In control cells ($n = 593$), branched microglia predominated, which morphologically showed a round cell body, with several branches and a weak signal with the iba-1 marker. The application of MCM ($n = 438$), HIS 100 μM ($n = 421$), and ATP 10 nM ($n = 618$) increased the rate of microglial activation. Preincubation with ketotifen ($n = 390$) or PPADS ($n = 404$) did not decrease MCM-mediated microglial activation. C) Potentiation of phagocytosis by MCM and HIS 100 μM at 48 h. ATP 10 nM induced no effect. Preincubation with ketotifen or PPADS did not significantly reduce the potentiation of MCM-induced phagocytosis. However, ketotifen inhibited the capture of beads induced by histamine. D) The rate of phagocytosis in ramified cells under control conditions is very low and was not affected by any treatment. E) The rate of phagocytosis in activated cells under control conditions is high and increased more when MCM or HIS was applied. ATP 10 nM reduced the number of phagocytosed beads compared to the control. Ketotifen but not PPADS inhibited histamine and MCM-mediated phagocytosis. Values (mean ± S.E.M) were calculated from three independent culturing experiments, using the Mann-Whitney rank sum test. Statistically significant from controls cells ($^{*}p < 0.05$; $^{**}p < 0.01$; $^{***}p < 0.001$). Statistically significant from MCM-treated cells ($^{\#\#}p < 0.01$). Statistically significant from histamine-treated cells ($^{\&}p < 0.05$; $^{\&\&\&}p < 0.001$). Scale bar 20 μm. (For interpretation of the references to colour in this figure legend, the reader is referred to the web version of this article.)

Table 1
Iba1 intensity and morphological changes in activated cells induced by different treatments.

	Iba1 intensity (au)	Area (μm^2)	Perimeter (μm)
Control ($n = 155$)	43.9 ± 2.3	67.76 ± 7.0	47.8 ± 2.5
MCM ($n = 169$)	32.2 ± 1.4 ***	103 ± 6.5***	65.9 ± 3***
HIS 100 μM ($n = 129$)	42.3 ± 2	113.11 ± 11.3***	74.2 ± 3.8***
ATP 10 nM ($n = 389$)	47.3 ± 1.5	65.8 ± 3.7	46.2 ± 1.6
MCM + KET ($n = 213$)	35 ± 1.3**	92.6 ± 5.4***	64.4 ± 2.4***
MCM + PPADS ($n = 110$)	40.3 ± 4	116.5 ± 9.1***	71.1 ± 2.8***
HIS + KET ($n = 121$)	44.8 ± 1.6	78.38 ± 4.9	53.3 ± 2.5

Statistically significant from control cells ($^{**}p < 0.01$; $^{***}p < 0.001$). Values (mean ± S.E.M) were calculated from three independent culture experiments, using the Mann-Whitney rank sum test.

3.5. Effect of ketotifen on single vesicle exocytosis

Fig. 4A shows activated microglia cells labeled with quinacrine monitored by epifluorescence. Punctate staining results from vesicular accumulation of the dye. Vesicles spontaneously lost their fluorescence (Supplementary video 1). These events can be interpreted as the release of quinacrine (and, presumably, ATP) from the vesicles into extracellular space [25]. First, to study exocytosis of quinacrine-stained vesicles, the changes in fluorescence intensity of individual vesicles were analyzed at 37 °C under basal conditions for a total observation time of 20 min. Fig. 4B represents sequential images of three quinacrine-stained vesicles showing the time course of changes in fluorescence intensity. There was a slow loss of fluorescence, as expected from the discharge of dye, when the vesicle fused with the plasma membrane, which was immediately preceded by an increase in fluorescence (indicated by arrows). This is presented graphically in Fig. 4C. Thus, these two processes of gain and loss of fluorescence are coupled or related. Fig. 4D shows activated microglia labeled with quinacrine in the presence of ketotifen. In this case, the vesicles manifested a more abrupt loss of fluorescence without a previous increment (Fig. E, F). (Supplementary video 2).

3.6. Ketotifen decreases vesicular exocytotic release by inhibiting vesicle acidification

In vitro, quinacrine accumulates in organelles upon imposing within an acidic transmembranous pH gradient (pH) and it is demonstrated that the accumulation of vesicular quinacrine is due to pH-driven concentration across membranes as an amphipathic amine [26]. Therefore, we wanted to determine whether the increase in fluorescence in quinacrine-loaded microglial vesicles could be a consequence of the increase in vesicular acidification.

Fig. 5A shows a representative example of the time course of a quinacrine loaded vesicle in a control activated cell. We measured three parameters for the quinacrine events: the transient increase in fluorescence preceding release (Rise), the time required to reach the maximum peak (Time to peak) and the amount of fluorescence released (Release). In addition, the decline of fluorescence could be fitted to a single or double decreasing exponential function (τ_1 and τ_2). The histogram of Time to peak was fitted to a Gaussian and showed a peak near 2 min, suggesting this time is frequently required to get the acidic pH into vesicles suitable for fusion to occur (Fig. 5B). However, the distribution also showed 14 % of events with a rapid increase in fluorescence (<30 s), like flashes (see supplementary video1). We next examined the change during the Rise and found that most events had an elevation of 22 % in fluorescence (Fig. 5C). Incubation with ketotifen completely inhibited the increase in vesicle fluorescence (Fig. 5D), as occurred with bafilomycin A1 (data not shown). These results suggest that ketotifen also inhibits vesicle acidification. On the other hand, we calculated the fraction of dye released during exocytosis over the total dye stored in single vesicle. The frequency histograms of the release fraction showed a shift from the most frequent value of 69.3 % in controls to 37.9 % in treated cells (Fig. 5E, F). On average, 69.1 ± 0.91 % and 44.15 ± 1.3 % of quinacrine fluorescence is released from vesicles in control and ketotifen treated cells, respectively (Fig. 5G), indicating that a greater fraction of vesicle content (~25 %) is released from control cells than from ketotifen-treated cells. Interestingly, the fluorescence decreased during vesicle release in the same proportion to the inhibition induced by ketotifen in the rise phase (control: 23.6 ± 1.1 %; KET: 1.2 ± 0.1 %). In general, the total release of individual exocytotic events is correlated with the data measured at the cellular level (Fig. 3G).

In addition, there is a linear relationship between maximum fluorescence and release from each vesicle in both control and treated cells (Fig. 5H). This suggests that the discharge of the vesicle content is highly dependent on the accumulation of quinacrine and proportionately, the ΔpH. However, comparatively, for the same start fluorescence, ketotifen reduced the amount of released content from each single fusion event.

The frequency distributions of decay time constants in secretory vesicles can be well fitted to a single (50.4 % of vesicles) or double (49.6 % of vesicles) exponential function. Vesicles that showed a double decay time course had time constants of 0.63 ± 0.06 min and 8.76 ± 1.76 min on average while vesicles that exhibited a single release kinetic had a τ of 1.29 ± 0.10 min (Fig. 5I). The fusion kinetics from the vesicles of cells treated with ketotifen was fitted to a fast single exponential with a τ of 0.73 ± 0.11 min (Fig. 5J).

4. Discussion

In this work, we show that ketotifen can be a valuable tool for microglial stabilization, especially when microglial activation is enhanced by MC degranulation. Our results demonstrate that MCM is an important activator of microglia, leading changes in microglial morphology, increasing the presence of the amoeboid phenotype (from 23 % to 50 %) that considerably differs from the homeostatic ramified phenotype, so called resting (Fig. 2B). This effect supports the fundamental role of the MC in neuroinflammation and is probably due to the activation of histamine receptors, since a potent cytosolic calcium

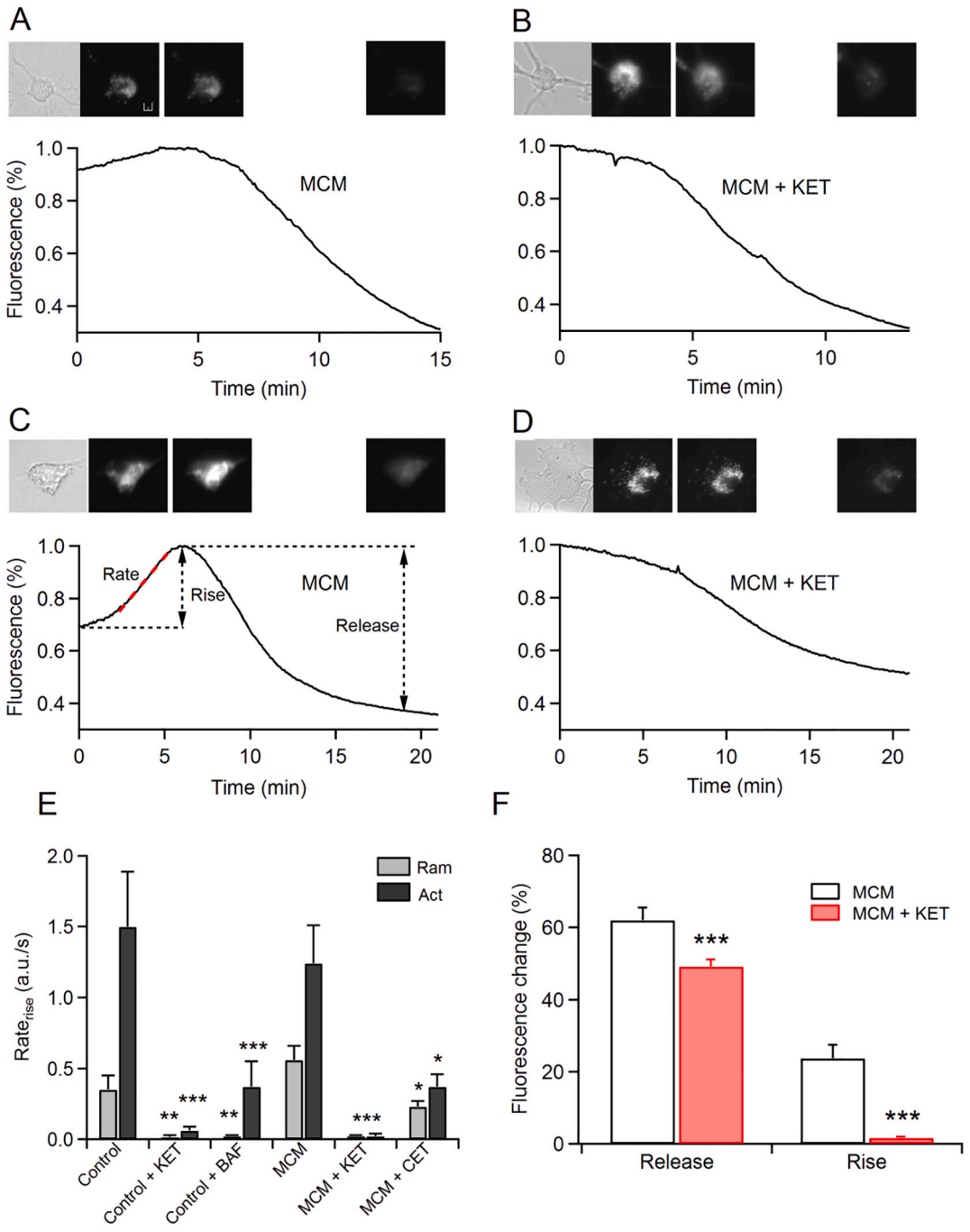

Fig. 3. Visualization of quinacrine fluorescence during exocytosis in microglia. A-B) Time courses of fluorescence in ramified microglia cells stimulated with MCM (A) and MCM after incubation for 10 min with ketotifen (MCM + KET) (B). The upper panels show a phase contrast image and 3 epifluorescence images at the beginning, middle and end of the records. The graphs show cell fluorescence signals as a percentage of the maximum values. C-D) Time courses of fluorescence in activated microglia cells stimulated with MCM (C) and MCM after incubation for 10 min with ketotifen (D). Upper panels show a phase contrast image and 3 epifluorescence images at the beginning, middle and end of the records. The graphs show the cell fluorescence signals as a percentage of the maximum values. E) Rate of rise in global fluorescence in control (Ram = 17; Act = 35) and treated cells with ketotifen (Ram = 10; Act = 50), bafilomycin (Ram = 13; Act = 33), MCM (Ram = 43; Act = 23), MCM incubated 10 min with ketotifen (MCM + KET) (Ram = 13; Act = 25) and cetirizine (MCM + CET) (Ram = 24; Act = 27). The slope of the line that best fits the phase of increase in fluorescence was measured as shown in C. F) Percentage of change during rise and release in global fluorescence in treated cells with MCM (white bar) and MCM incubated with ketotifen (MCM + KET) (red bar). Statistically significant from MCM treated cells (*$p < 0.05$; **$p < 0.01$; ***p < 0.001). Values (mean ± S.E.M) were calculated from three independent culture experiments, using the Mann-Whitney rank sum test. (For interpretation of the references to colour in this figure legend, the reader is referred to the web version of this article.)

$[Ca^{2+}]_c$ signal is rapidly induced when histamine or MCM are applied (Fig. 1C, D). Histamine receptors are expressed in microglia and control microglial functions, including chemotaxis, migration, cytokine secretion, and phagocytosis. [27]. In the current work, ketotifen, a H1R antagonist, abolished the increase in $[Ca^{2+}]_i$ mediated by histamine suggesting that H1R alone is involved in this $[Ca^{2+}]_i$ transient. Ketotifen reduced >60 % of the signal mediated by MCM, leaving a signal like that induced by ATP (Fig. 1C, F). Otherwise, H1R is not involved in the morphological changes generated by MCM exclusively because this antagonist did not affect the activated microglia population (Fig. 2B),

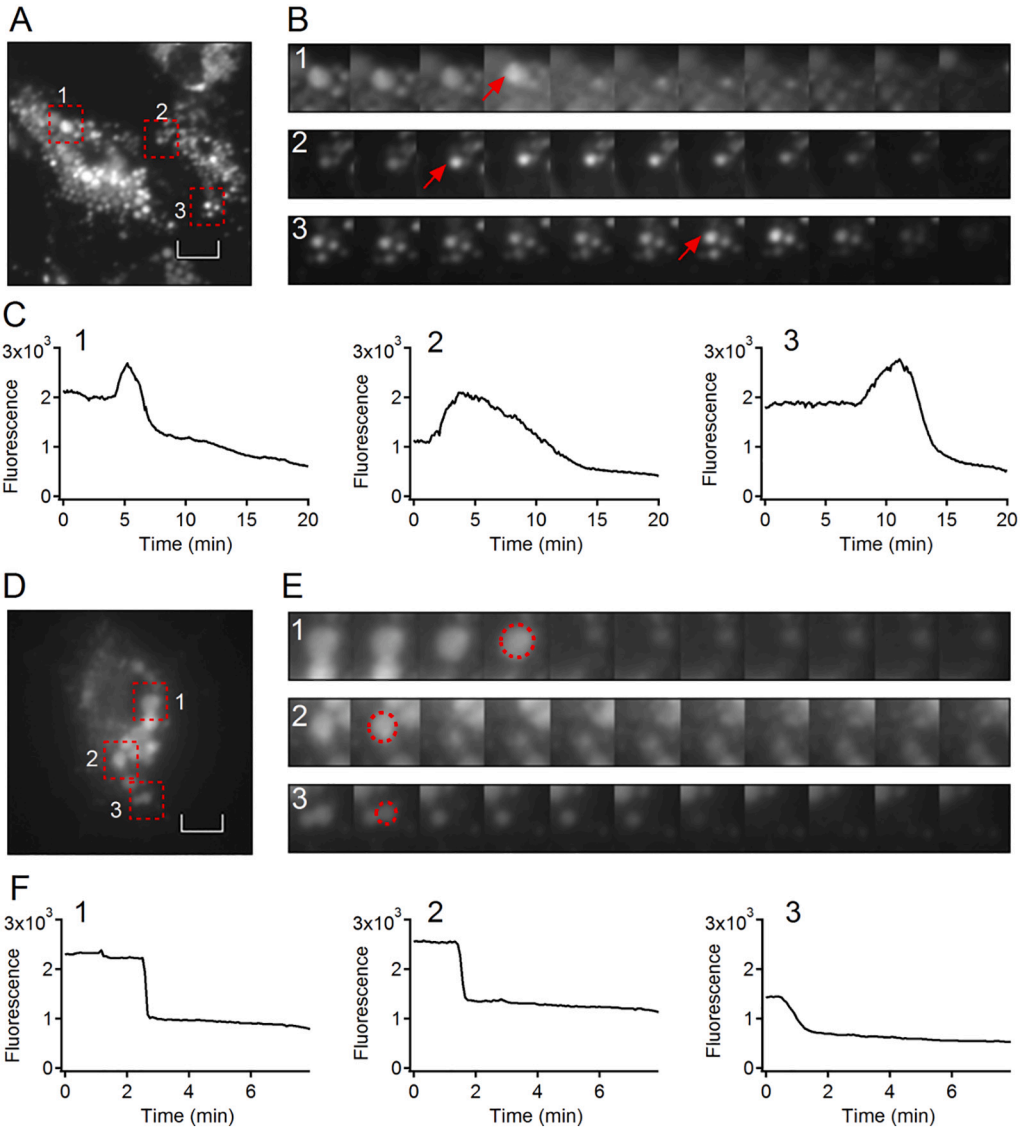

Fig. 4. Changes in fluorescence intensity of quinacrine-containing vesicles during exocytosis in control and ketotifen-treated cells. A) Image of cells stained with quinacrine with 3 regions of interest placed in selected vesicles. B) Sequential images of 3 quinacrine loaded vesicles showing the time course of fluorescence changes within ROI (each image every 100 s). Before the loss of fluorescence, an increase is observed, which is indicated by an arrow on the sequence. C) Time courses of fluorescence changes of vesicles indicated in B. The increase in fluorescence in each spot precedes a slow loss. D) Image of a single quinacrine stained cell incubated in the presence of ketotifen 100 μM. 3 regions of interest are placed on selected vesicles. E) Sequential images of 3 quinacrine loaded vesicles treated with ketotifen showing the time course of fluorescence changes within ROI (each image every 50 s). The fluorescence spots are outlined by dotted red circles in the image anterior to loss of fluorescence. No elevation was observed prior to the release. F) Time courses of fluorescence changes of vesicles indicated in E. Compared to control cells, a more abrupt loss of fluorescence occurs. Scale bar: 4 μm. (For interpretation of the references to colour in this figure legend, the reader is referred to the web version of this article.)

nor did it modify the perimeter or area of the cell (Table 1).

In total cells, MCM and histamine increased basal phagocytosis, a critical calcium-dependent function of microglia (Fig. 2C). The underlying mechanism appears to involve H1R since ketotifen partially decreased the effect of MCM. However, phagocytosis remained significantly elevated compared to the control. The involvement of H1R in phagocytosis has already been described [18].

Additionally, we wanted to determine the specific involvement of microglial phenotypes observed in our cultures in phagocytosis (ramified vs. activated). In a healthy brain, prevalent microglia are the ramified phenotype whose main functions are immune surveillance and synaptic pruning [28]. However, its role in phagocytosis is unclear. Our results showed that ramified microglia are competent in this process, but at a significantly lower level (<3 times) than the ameboid phenotype (Fig. 2D, E). In addition, the capture of beads by ramified cells was not altered by any stimulation (MCM, histamine, ATP). On the other hand, basal phagocytosis in activated microglia was increased two to three times by MCM and histamine, respectively, and ketotifen significantly inhibited it (Fig. 2E), suggesting that in part it is the greater ratio of activated/ramified cells in the presence of MCM that explains the higher overall rate even when ketotifen is present (Fig. 2C). Instead, ATP inhibited the engulfment of beads as previously reported [29].

Quinacrine is a fluorescent dye that has been used as a vital probe to visualize the vesicular storage of ATP, but recently, it was concluded that the accumulation of vesicular quinacrine is not due to a consequence of its interaction with ATP, but due to the concentration driven by pH across the membranes [26]. As a consequence, when the vesicular pH decreases, more quinacrine is accumulated and the fluorescence increases. We observed a global increase in cellular quinacrine fluorescence (Fig. 3A, C) that probably represents an increase in cellular acidification. Ketotifen totally inhibited this increase in fluorescence, while bafilomycin and cetirizine did it partially (Fig. 3E).

Acidification of secretory vesicles is required for the transport of small-molecule transmitters through specific transporters in vesicular membranes. The generator of the large electrochemical proton gradient, acidic and positive inside these organelles is the vacuolar-type ATPases [30]. In this manner, when the transmembrane pH gradient is increased, the driving force for the uptake of small molecules is enhanced and the content in secretory vesicles augments [31]. This pump is expressed in secretory organelles of all eukaryotes [32,33]. In human eosinophils it was proposed that granule acidification is a major step in solubilisation of major protein crystals, which are stored within the granule core, in preparation for degranulation and release of these toxic proteins [34]. Furthermore, it has been suggested that 'priming' insulin-containing secretory granules involves further acidification of the lumen of the granule [35]. In MCs, bafilomycin A1 treatment causes a robust increase

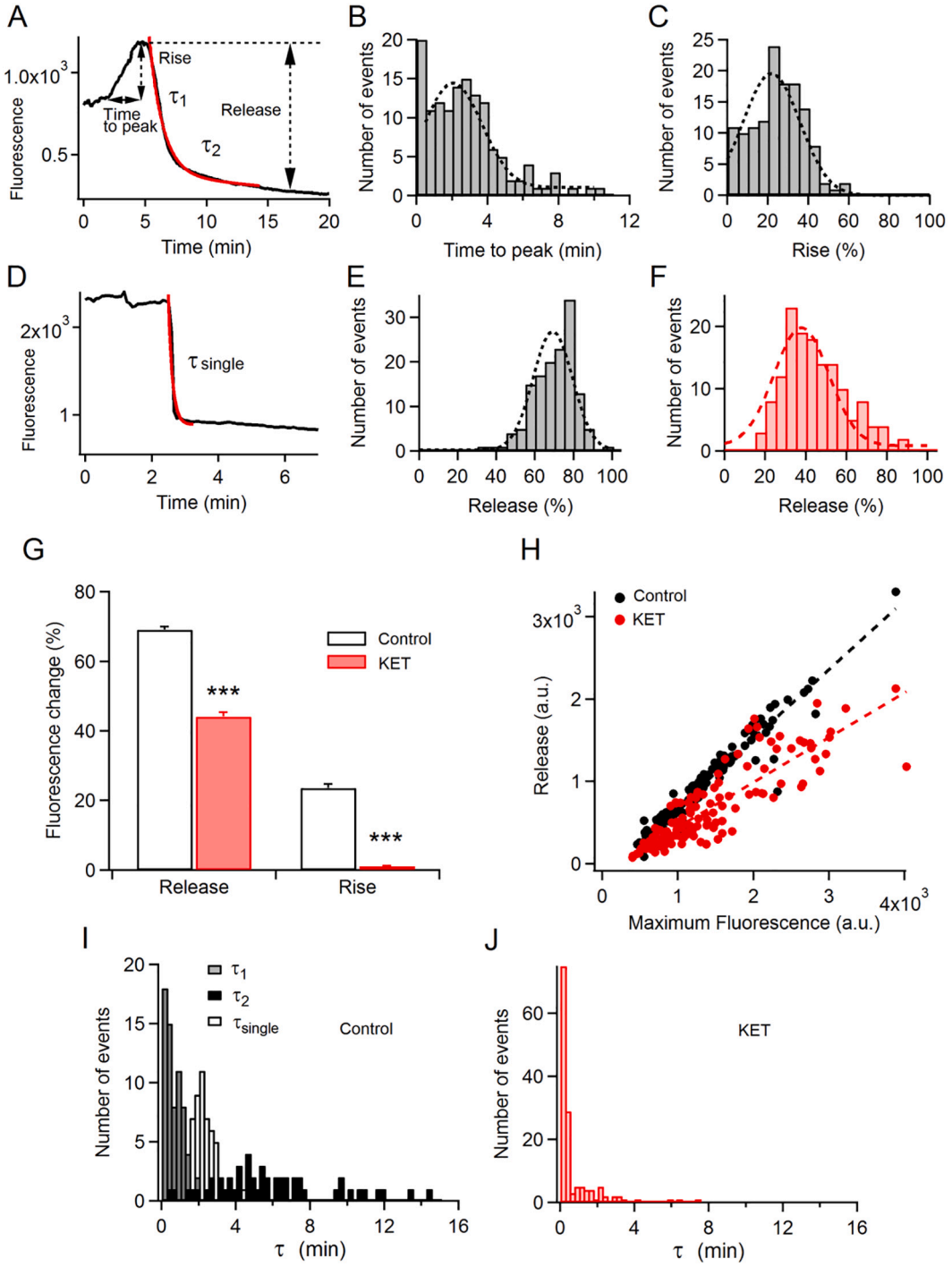

Fig. 5. Analysis of cargo release during exocytosis in control and ketotifen-treated microglia. A) Example of the time course of quinacrine fluorescence loss in a vesicle from control activated microglia. The parameters analyzed are the Time to peak and the increase in fluorescence (difference between the initial and the maximum fluorescence values). The kinetics of release was fitted to single or double exponential functions, providing the time constants τ_1 and τ_2. B) Distribution histogram of Time to peak of cargo release. C) Distribution histogram of fluorescence increase (in %) of single events. D) Example of the time course of quinacrine fluorescence in a vesicle from ketotifen-treated cell. E) Distribution histogram of the fraction of Release (%) of single events from control cells (grey bars). F) Distribution histogram of the fraction of release (%) of single events from cells treated with ketotifen (red bars). G) Fraction of Release and Rise (%) during single exocytotic events in control (white bar; $n = 140$) and ketotifen-treated cells (red bar; $n = 145$) (***$p < 0.001$). H) Correlation between the maximum and the loss of fluorescence of each single event obtained from control cells (black point) and cells treated with ketotifen (red points). I) Distribution histogram of time constants (τ_1, τ_2, τ_{single}) from fusion events in control cells. J) Distribution histogram of time constants (τ_1) from fusion events in ketotifen-treated cells. (For interpretation of the references to colour in this figure legend, the reader is referred to the web version of this article.)

in granule pH, aberrant processing of pro-carboxypeptidase A3, and a reduction in tryptase enzymatic activity and intracellular histamine [36]. Our experiments reveal that the pH of secretory organelles in microglia is not a steady variable but decreases just before vesicular fusion takes place, suggesting that acidification of the secretory pathway is under regulation and may favors the accumulation of solutes. Cell incubation with ketotifen or bafilomycin A1 inhibited fusion-associated vesicle acidification and, consequently, the fraction of quinacrine released by the vesicle was reduced a 25 % (Fig. 5H) indicating that this last stage of vesicle acidification may contribute to determine the extent of the inflammatory reaction mediated by microglia.

However, although in our experiments this last step of acidification is suppressed by ketotifen, many secretory vesicles are primed for exocytosis, and as previously reported, inhibition of V-ATPase activity by bafilomycin A1 was also not required for transmitter release [37]. In addition, vesicular pH plays a key role in modulating exocytotic kinetics [38] and V-ATPases are involved in control of neurotransmitter release and in exocytosis of secretory granules [39] [40]. It has been proposed the domain membrane of V-ATPase would allow the exocytotic machinery to discriminate fully loaded and acidified vesicles from vesicles undergoing transmitter reloading [39]. In our experiments, inhibition of intravesicular acidification with ketotifen decreased cargo discharge (Fig. 5G) supporting this hypothesis. Likely, this inhibitory mechanism did not involve a direct effect on V-ATPase activity, because of cetirizine, another H1R antagonist, also had a similar effect (Fig. 3E). Mechanisms regulating changes in vesicular pH remain unclear; however, there is substantial evidence indicating that pH is modified by the contents of phosphatidylinositol phosphate lipids of membranes [41] as well as the activation of protein kinase A pathway [42].

We observed distinct types of secretory vesicles based on the kinetics of fluorescence decay (Fig. 5I). Vesicles whose kinetic is adjusted to a single and others better fitted to a double exponential function. When a single exocytotic event is slow, it is plausible that a fusion mechanism known as “kiss-and-run” occurs [43]. The vesicle opens and closes through a narrow fusion pore. Repetitive “kiss-and-run” fusion event at brief intervals allows for slow release of mediators [44]. Besides, when the fusion pore transiently was closed, the vesicle may re-acidify and reload. Both processes of fusion and re-acidification could explain the two kinetics of fluorescence release at the single vesicle. Nevertheless, discharge is faster in the presence of ketotifen compared to the control (Fig. 5J). Ketotifen eliminates the slower exocytotic fusion and only vesicles that fuse quickly ($\tau = 0.73 \pm 0.11$ min) remains, probably through the abrupt expansion of the fusion pore that induces the rapid loss of contents [45]. The dynamics of the fusion pore as well as the mode of exocytosis is regulated by intracellular calcium [46,47]. The accumulation of large concentrations of calcium in secretory vesicles occurs and is also dependent on acidification of the vesicle [48]. Thus, disrupting the pH gradient promotes the leakage of vesicular calcium that affects exocytosis [49]. Histamine can also mobilize the free Ca^{2+} fraction in vesicles [50]. Therefore, changes in vesicular calcium would modify vesicle acidification and the dynamics of the exocytotic fusion pore and, consequently, H1R antagonists would affect these processes.

Attenuating secretory paths to inhibit inflammatory mediators and controlling microglial inflammatory response are considered therapeutic strategies for treating neurodegenerative diseases [51,52]. Therefore, due to its known stabilizing effect on MCs by reducing histamine release and in addition, to its direct action on microglia, ketotifen can be considered a dual therapeutic tool. Thus, ketotifen, a safe drug that crosses the blood-brain barrier, has been described to improve patients with multiple sclerosis [53], a neurodegenerative disease in which both MCs and microglia play a crucial role.

5. Conclusion

Ketotifen can be considered a microglial stabilizer, weakening its overactivated phenotype to a less aggressive state. It could inhibit the microglia by potentially reducing the release of dangerous molecules and mediators contained in secretory organelles that can be harmful to the inflamed brain.

Supplementary data to this article can be found online at https://doi.org/10.1016/j.lfs.2023.121537.

Funding

This work was supported by the financial assistance from the Junta de Andalucía (BIO-236).

CRediT authorship contribution statement

María Pilar Ramírez-Ponce: Conceptualization, Formal analysis, Investigation, Writing – original draft. **Juan Antonio Flores:** Conceptualization, Formal analysis, Methodology, Investigation. **Lorenzo Barrella:** Methodology, Investigation. **Eva Alés:** Conceptualization, Formal analysis, Investigation, Writing – original draft.

Declaration of competing interest

The authors declare that there are not conflicts of interest.

Acknowledgements

We thank Mª. Dolores Maldonado for her technical support in ELISA measurements.

References

[1] A. Nimmerjahn, F. Kirchhoff, F. Helmchen, Resting microglial cells are highly dynamic surveillants of brain parenchyma in vivo, Science 308 (2005) 1314–1318, https://doi.org/10.1126/SCIENCE.1110647.
[2] D. Soulet, S. Rivest, Microglia, Curr. Biol. 18 (2008), https://doi.org/10.1016/J.CUB.2008.04.047.
[3] J.K. Sandhu, M. Kulka, Decoding mast cell-microglia communication in neurodegenerative diseases, Int. J. Mol. Sci. 22 (2021) 1–22, https://doi.org/10.3390/IJMS22031093.
[4] M.Y. Wendimu, S.B. Hooks, Microglia phenotypes in aging and neurodegenerative diseases, Cells. 11 (2022), https://doi.org/10.3390/CELLS11132091.
[5] F. Florenzano, M. Bentivoglio, Degranulation, density, and distribution of mast cells in the rat thalamus: a light and electron microscopic study in basal conditions and after intracerebroventricular administration of nerve growth factor - PubMed, J. Comp. Neurol. (2000) 651–669 (accessed October 10, 2022), https://pubmed.ncbi.nlm.nih.gov/10931487/.
[6] M. Khalil, J. Ronda, M. Weintraub, K. Jain, R. Silver, A.J. Silverman, Brain mast cell relationship to neurovasculature during development, Brain Res. 1171 (2007) 18–29, https://doi.org/10.1016/J.BRAINRES.2007.07.034.
[7] D. Maslinska, M. Laure-Kamionowska, K.T. Maslinski, M. Gujski, S. Maslinski, Distribution of tryptase-containing mast cells and metallothionein reactive astrocytes in human brains with amyloid deposits, Inflamm. Res., Inflamm Res (2007), https://doi.org/10.1007/s00011-006-0508-8.
[8] P.A. Harcha, A. Vargas, C. Yi, A.A. Koulakoff, C. Giaume, J.C. Sáez, Hemichannels are required for amyloid β-peptide-induced degranulation and are activated in brain mast cells of APPswe/PS1dE9 mice, J. Neurosci. 35 (2015) 9526–9538, https://doi.org/10.1523/JNEUROSCI.3686-14.2015.
[9] Y. Jin, A.J. Silverman, S.J. Vannucci, Mast cells are early responders after hypoxia-ischemia in immature rat brain, Stroke 40 (2009) 3107–3112, https://doi.org/10.1161/STROKEAHA.109.549691.
[10] A.M. Dvorak, New aspects of mast cell biology, Int. Arch. Allergy Immunol. 114 (1997) 1–9, https://doi.org/10.1159/000237635.
[11] S.J. Galli, S. Nakae, M. Tsai, Mast cells in the development of adaptive immune responses, Nat. Immunol. 6 (2005) 135–142, https://doi.org/10.1038/ni1158.
[12] X. Zhang, Y. Wang, H. Dong, Y. Xu, S. Zhang, Induction of microglial activation by mediators released from mast cells, Cell. Physiol. Biochem. 38 (2016) 1520–1531, https://doi.org/10.1159/000443093.
[13] H. Dong, X. Zhang, Y. Qian, Mast cells and neuroinflammation, Med. Sci. Monit. Basic Res. 20 (2014) 200–206, https://doi.org/10.12659/MSMBR.893093.
[14] H. Dong, Y. Wang, X. Zhang, X. Zhang, Y. Qian, H. Ding, S. Zhang, Stabilization of brain mast cells alleviates LPS-induced neuroinflammation by inhibiting microglia activation, Front. Cell. Neurosci. 13 (2019), https://doi.org/10.3389/FNCEL.2019.00191.
[15] X. Zhang, W. Wu, Z. Zheng, L. Li, J. Chen, J. Zhong, L. Zhao, J. Chen, Z. Wang, F. Meng, Mast cell stabilizer disodium cromoglycate improves long-term cognitive impairment after general anesthesia exposure in neonatal mice, Front. Neurosci. 16 (2022), https://doi.org/10.3389/FNINS.2022.990333.

[16] J. Zhu, C. Qu, X. Lu, S. Zhang, Activation of microglia by histamine and substance P, Cell. Physiol. Biochem. 34 (2014) 768–780, https://doi.org/10.1159/000363041.
[17] M.P. Ramírez-Ponce, A. Sola-García, S. Balseiro-Gómez, M.D. Maldonado, J. Acosta, E. Alés, J.A. Flores, Mast cell changes the phenotype of microglia via histamine and ATP, Cell. Physiol. Biochem. 55 (2021) 17–32, https://doi.org/10.33594/000000324.
[18] S.M. Rocha, T. Saraiva, A.C. Cristóvão, R. Ferreira, T. Santos, M. Esteves, C. Saraiva, G. Je, L. Cortes, J. Valero, G. Alves, A. Klibanov, Y.-S. Kim, L. Bernardino, Histamine induces microglia activation and dopaminergic neuronal toxicity via H1 receptor activation, J. Neuroinflamm. 13 (2016) 137, https://doi.org/10.1186/s12974-016-0600-0.
[19] J. Kim, J.H. Song, Inhibitory effects of antihistamines, diphenhydramine and chlorpheniramine, on proton currents in BV2 microglial cells, Eur. J. Pharmacol. 798 (2017) 122–128, https://doi.org/10.1016/J.EJPHAR.2017.01.032.
[20] P. Lacy, J.L. Stow, Cytokine release from innate immune cells: association with diverse membrane trafficking pathways, Blood 118 (2011) 9–18, https://doi.org/10.1182/BLOOD-2010-08-265892.
[21] A. Baba, M. Tachi, Y. Ejima, Y. Endo, H. Toyama, M. Matsubara, K. Saito, M. Yamauchi, C. Miura, I. Kazama, Anti-allergic drugs tranilast and ketotifen dose-dependently exert mast cell-stabilizing properties, Cell. Physiol. Biochem. 38 (2016) 15–27, https://doi.org/10.1159/000438605.
[22] J.A. Flores, M.P. Ramírez-Ponce, M.Á. Montes, S. Balseiro-Gómez, J. Acosta, G. Álvarez De Toledo, E. Alés, Proteoglycans involved in bidirectional communication between mast cells and hippocampal neurons, J. Neuroinflamm. 16 (2019), https://doi.org/10.1186/s12974-019-1504-6.
[23] H. Lian, E. Roy, H. Zheng, Microglial phagocytosis assay, Bio-Protocol. 6 (2016), https://doi.org/10.21769/bioprotoc.1988.
[24] A. Pierzyńska-Mach, P.A. Janowski, J.W. Dobrucki, Evaluation of acridine orange, LysoTracker red, and quinacrine as fluorescent probes for long-term tracking of acidic vesicles, Cytometry. A 85 (2014) 729–737, https://doi.org/10.1002/CYTO.A.22495.
[25] K. Striedinger, P. Meda, E. Scemes, Exocytosis of ATP from astrocyte progenitors modulates spontaneous Ca2+ oscillations and cell migration, Glia. 55 (2007) 652–662, https://doi.org/10.1002/GLIA.20494.
[26] N. Hasuzawa, S. Moriyama, L. Wang, A. Nagayama, K. Ashida, Y. Moriyama, M. Nomura, Quinacrine is not a vital fluorescent probe for vesicular ATP storage, Purinergic Signal 17 (2021) 725–735, https://doi.org/10.1007/S11302-021-09820-8.
[27] L. Bernardino, Histamine in the crosstalk between innate immune cells and neurons: relevance for brain homeostasis and disease, Curr. Top. Behav. Neurosci. 59 (2022), https://doi.org/10.1007/7854_2021_235.
[28] E.E. Benarroch, Microglia: multiple roles in surveillance, circuit shaping, and response to injury, Neurology 81 (2013) 1079–1088, https://doi.org/10.1212/WNL.0B013E3182A4A577.
[29] K.M. Fang, C.S. Yang, S.H. Sun, S.F. Tzeng, Microglial phagocytosis attenuated by short-term exposure to exogenous ATP through P2X receptor action, J. Neurochem. 111 (2009) 1225–1237, https://doi.org/10.1111/J.1471-4159.2009.06409.X.
[30] R.G. Johnson, Proton pumps and chemiosmotic coupling as a generalized mechanism for neurotransmitter and hormone transport, Ann. N. Y. Acad. Sci. 493 (1987) 162–177, https://doi.org/10.1111/J.1749-6632.1987.TB27198.X.
[31] E.N. Pothos, E. Mosharov, K.P. Liu, W. Setlik, M. Haburcak, G. Baldini, M. D. Gershon, H. Tamir, D. Sulzer, Stimulation-dependent regulation of the pH, volume and quantal size of bovine and rodent secretory vesicles, J. Physiol. 542 (2002) 453–476, https://doi.org/10.1113/JPHYSIOL.2002.018630.
[32] M.E. Finbow, M.A. Harrison, The vacuolar H+-ATPase: a universal proton pump of eukaryotes, Biochem. J. 324 (Pt 3) (1997) 697–712, https://doi.org/10.1042/BJ3240697.
[33] R.H. Edwards, The neurotransmitter cycle and quantal size, Neuron 55 (2007) 835–858, https://doi.org/10.1016/J.NEURON.2007.09.001.
[34] J.L. Bankers-Fulbright, G.M. Kephart, K.R. Bartemes, H. Kita, S.M. O'Grady, Platelet-activating factor stimulates cytoplasmic alkalinization and granule acidification in human eosinophils, J. Cell Sci. 117 (2004) 5749–5757, https://doi.org/10.1242/JCS.01498.
[35] S. Barg, P. Huang, L. Eliasson, D.J. Nelson, S. Obermüller, P. Rorsman, F. Thévenod, E. Renström, Priming of insulin granules for exocytosis by granular Cl(-) uptake and acidification, J. Cell Sci. 114 (2001) 2145–2154, https://doi.org/10.1242/JCS.114.11.2145.
[36] G. Pejler, J.M. Hu Frisk, D. Sjöström, A. Paivandy, H. Öhrvik, Acidic pH is essential for maintaining mast cell secretory granule homeostasis, Cell Death Dis. 8 (2017), https://doi.org/10.1038/CDDIS.2017.206.
[37] M.A. Cousin, D.G. Nicholls, Synaptic vesicle recycling in cultured cerebellar granule cells: role of vesicular acidification and refilling, J. Neurochem. 69 (1997) 1927–1935, https://doi.org/10.1046/J.1471-4159.1997.69051927.X.
[38] M. Camacho, J.D. Machado, M.S. Montesinos, M. Criado, R. Borges, Intragranular pH rapidly modulates exocytosis in adrenal chromaffin cells, J. Neurochem. 96 (2006) 324–334, https://doi.org/10.1111/J.1471-4159.2005.03526.X.
[39] S. Poëa-Guyon, M.R. Ammar, M. Erard, M. Amar, A.W. Moreau, P. Fossier, V. Gleize, N. Vitale, N. Morel, The V-ATPase membrane domain is a sensor of granular pH that controls the exocytotic machinery, J. Cell Biol. 203 (2013) 283–298, https://doi.org/10.1083/JCB.201303104.
[40] N. Morel, S. Poëa-Guyon, The membrane domain of vacuolar H(+)ATPase: a crucial player in neurotransmitter exocytotic release, Cell. Mol. Life Sci. 72 (2015) 2561–2573, https://doi.org/10.1007/S00018-015-1886-2.
[41] S. Banerjee, P.M. Kane, Regulation of V-ATPase activity and organelle pH by phosphatidylinositol phosphate lipids, Front. Cell Dev. Biol. 8 (2020), https://doi.org/10.3389/FCELL.2020.00510.
[42] L.S. Tompkins, K.D. Nullmeyer, S.M. Murphy, C.S. Weber, R.M. Lynch, Regulation of secretory granule pH in insulin-secreting cells, Am. J. Physiol. Cell Physiol. 283 (2002), https://doi.org/10.1152/AJPCELL.01066.2000.
[43] G. Álvarez de Toledo, M.Á. Montes, P. Montenegro, R. Borges, Phases of the exocytotic fusion pore, FEBS Lett. 592 (2018) 3532–3541, https://doi.org/10.1002/1873-3468.13234.
[44] X. Qin, R.W. Tsien, H. Park, Real-time three-dimensional tracking of single synaptic vesicles reveals that synaptic vesicles undergoing kiss-and-run fusion remain close to their original fusion site before reuse, Biochem. Biophys. Res. Commun. 514 (2019) 1004–1008, https://doi.org/10.1016/J.BBRC.2019.05.043.
[45] P. Ñeco, C. Fernández-Peruchena, S. Navas, L.M. Gutiérrez, G. Álvarez De Toledo, E. Alés, Myosin II contributes to fusion pore expansion during exocytosis, J. Biol. Chem. 283 (2008) 10949–10957, https://doi.org/10.1074/JBC.M709058200.
[46] R. Fernández-Chacón, G.A. de Toledo, Cytosolic calcium facilitates release of secretory products after exocytotic vesicle fusion, FEBS Lett. 363 (1995) 221–225, https://doi.org/10.1016/0014-5793(95)00319-5.
[47] E. Alés, L. Tabares, J.M. Poyato, V. Valero, M. Lindau, G.A. De Toledo, High calcium concentrations shift the mode of exocytosis to the kiss-and-run mechanism, Nat. Cell Biol. 1 (1999) 40–44, https://doi.org/10.1038/9012.
[48] A. Moreno, C.D. Lobatón, J. SantoDomingo, L. Vay, E. Hernández-SanMiguel, R. Rizzuto, M. Montero, J. Alvarez, Calcium dynamics in catecholamine-containing secretory vesicles, Cell Calcium 37 (2005) 555–564, https://doi.org/10.1016/J.CECA.2005.02.002.
[49] R. Borges, N. Domínguez, J. Estévez-Herrera, D. Pereda, J.D. Machado, Vesicular Ca(2+) mediates granule motion and exocytosis, Cell Calcium 51 (2012) 338–341, https://doi.org/10.1016/J.CECA.2011.12.009.
[50] J. SantoDomingo, L. Vay, M. Camacho, E. Hernández-SanMiguel, R.I. Fonteriz, C. D. Lobatón, M. Montero, A. Moreno, J. Alvarez, Calcium dynamics in bovine adrenal medulla chromaffin cell secretory granules, Eur. J. Neurosci. 28 (2008) 1265–1274, https://doi.org/10.1111/J.1460-9568.2008.06440.X.
[51] Y.J. Wang, A. Monteagudo, M.A. Downey, P.G. Ashton-Rickardt, D.R. Elmaleh, Cromolyn inhibits the secretion of inflammatory cytokines by human microglia (HMC3), Sci. Rep. 11 (2021), https://doi.org/10.1038/S41598-021-85702-8.
[52] G. Galvani, N. Mottolese, L. Gennaccaro, M. Loi, G. Medici, M. Tassinari, C. Fuchs, E. Ciani, S. Trazzi, Inhibition of microglia overactivation restores neuronal survival in a mouse model of CDKL5 deficiency disorder, J. Neuroinflamm. 18 (2021), https://doi.org/10.1186/S12974-021-02204-0.
[53] K.H. Pinke, S.F.G. Zorzella-Pezavento, T.F. de Campos Fraga-Silva, L.A.N. Mimura, L.R.C. de Oliveira, L.L.W. Ishikawa, A.A.H. Fernandes, V.S. Lara, A. Sartori, Calming down mast cells with ketotifen: a potential strategy for multiple sclerosis therapy? Neurotherapeutics 17 (2020) 218–234, https://doi.org/10.1007/S13311-019-00775-8.